ELSEVIER

Journal of Non-Crystalline Solids 189 (1995) 218–226

JOURNAL OF NON-CRYSTALLINE SOLIDS

Pr^{3+}-doped fluoride glasses

W. Seeber [a,*], E.A. Downing [b], L. Hesselink [b], M.M. Fejer [c], D. Ehrt [a]

[a] *University of Jena, Otto-Schott-Institute, Fraunhoferstr. 6, D-07743 Jena, Germany*
[b] *Stanford University, Department of Electrical Engineering, Stanford, CA 94305, USA*
[c] *Stanford University, Department of Applied Physics, Stanford, CA 94305, USA*

Received 13 January 1995; revised 14 March 1995

Abstract

Fluoride-based glasses are potential host materials for fiber lasers, amplifiers and solid state three-dimensional (3D) displays. Fluorozirconate (ZrF_4–BaF_2–LaF_3–AlF_3–NaF), fluoride phosphate (AlF_3–SrF_2–CaF_2–MgF_2–P_2O_5) and fluoroindate (InF_3–ZnF_2–BaF_2–GaF_3–PbF_2–REF_3–SrF_2–NaF–CaF_2) glasses were investigated in terms of their absorption and crystallization properties to compare their potential to be used as optical devices. Phonon sideband (PSB) measurements were employed to determine the local vibration behavior of the rare earth (RE) ion sites. A modified Judd–Ofelt treatment allows the description of transition probabilities between Pr^{3+} energy levels, including error estimates for the fitted parameters Ω_t. In the investigated fluoroindate glasses melted in vitreous carbon crucibles using a reactive atmosphere, processing fanlike crystals composed of Sr and RE fluorides caused manufacturing problems.

1. Introduction

Fluoride-based glasses are currently under investigation because of their potential use as high-efficiency optical devices, e.g. fiber and bulk lasers, fiber amplifiers and solid state 3D display applications ([1–8] and references therein). Among the various compositions of vitreous fluoride materials, only fluorozirconate glasses have been reproducibly drawn into high-quality optical fibers [9], despite great efforts since the discovery of fluoride glasses [10]. The investigations of new InF_3-based glasses containing Pb, Cd, Na and Gd fluorides [11] and the manufacturing of suitable preforms for fiber drawing [12] appear promising for improved devices. For practical commercial applications, the following goals in the development of fluoride-based glasses remain:

- to increase the up-conversion efficiencies and the radiative transition probabilities of rare earth (RE) dopant ions through the selection of families of glasses with low multiphonon emission rates,
- to improve the crystallization stability and manufacture of bulk samples > 1 cm^3,
- to increase the IR transparency and chemical durability,
- to avoid the release of toxic or otherwise hazardous compounds from the material,
- to develop less expensive manufacturing methods, and
- to control and measure trace impurities in all steps of manufacturing.

For the investigations discussed here we chose the following three fluoride-based glass families: fluo-

* Tel: +49-3641 636 105. Telefax: +49-3641 361 72. E-mail: cws@rz.uni.jena.de

SSDI 0022-3093(95)00241-3

rozirconates, because of their well-known fiber-drawing capability; fluoride phosphates (FPs), because they are comparatively easy and inexpensive to produce in excellent optical quality; and fluoroindates, because of their potential to increase the up-conversion efficiency which is intrinsically limited in fluorozirconates. Our goals were to investigate the fabrication requirements, the spectroscopic properties and the crystallization behavior of these different glass systems and to evaluate their potential for further applications. The Pr^{3+} energy level scheme is especially useful for applications that require 1.3 μm amplification or two-step photoexcitation/up-conversion fluorescence [7,13]. As a probe of the local vibration behavior around RE sites we used Eu^{3+}-doped samples and employed the well-known phonon sideband (PSB) technique [14].

The optical properties of Pr^{3+} have been studied in numerous hosts: e.g. in water [15], in crystals [16–18], in glasses [19–21] and as 'free ions' [22]. To describe the transition probabilities between the Pr^{3+} $^1G_4$ level to higher levels, the well-known Judd–Ofelt parameters Ω_t [23,24] were derived empirically from measurements of integrated absorption cross sections [16,17]. These probabilities provide insights into the two-step photoexcitation properties of Pr^{3+}.

2. Experimental

Glasses were prepared by using powders or crystals of ZrF_4, AlF_3, InF_3, GaF_3, CaF_2, SrF_2, BaF_2, ZnF_2, LiF, NaF, $Ba(PO_3)_2$, $Sr(PO_3)_2$ and REF_3 (RE: Pr, Eu, Gd, Yb or Lu) of the highest available purity as starting materials. Table 1 shows typical batch compositions.

For the preparation of fluorozirconates and fluoroindates, batches of compounds (up to 10 g) were melted in vitreous carbon crucibles using a reactive atmosphere processing technique (chlorine gas). The temperature was gradually increased to melting (1050–1100 K). Finally, fining was carried out in the same way as for standard fluoride glasses ([10,12] and references therein).

For the preparation of fluoride phosphates, batches of the compounds (up to 100 g) were melted in covered platinum crucibles in the temperature range 1000–1400 depending on the phosphate content. The liquids were poured into graphite molds and cooled at a rate of 2 K/min to room temperature. The samples were cut and then polished with diamond paste. A typical sample size for spectroscopic investigations was $10 \times 10 \times 5$ mm^3.

Absorption spectra were obtained with a double-beam UV-VIS-NIR spectrometer (Shimadzu model

Table 1
Typical starting compositions, measured densities and estimated Pr^{3+} concentrations of investigated glasses

Glass	System	Composition (mol%)	Melting range (K)	ρ (g/cm^3)	Pr^{3+} conc. for $x = 0.5$ (ions/cm^3)
Z-1	Fluorozirconate	$(53 - x)$ ZrF_4–20 BaF_2–4LaF_3–3 AlF_3–20 NaF–x REF_3 ($x = 0, 0.5, 2.0$; RE = Pr, Eu)	1050–1100	4.30	0.9×10^{20}
I-1	Fluoroindate	20 InF_3–18 ZnF_2–15 BaF_2–12 GaF_3–10 PbF_2–7 YbF_3–5 SrF_2–5 NaF–3 GdF_3–3 CaF_2–$(2 - x)$ LuF_3–x REF_3 ($x = 0, 0.5, 2.0$; RE = Pr, Eu)	1050–1100	5.30	1.0×10^{20}
FP-3	Fluoride phosphate	37 AlF_3–10 MgF_2–28 CaF_2–22 SrF_2–3 $Sr(PO_3)_2$–x REF_3 ($x = 0, 0.5, 2.0$; RE = Pr, Eu	1000–1200	3.50	1.1×10^{20}
FP-10	Fluoride phosphate	34 AlF_3–10 MgF_2–30 CaF_2–16 SrF_2–10 $Sr(PO_3)_2$–x REF_3 ($x = 0, 0.5, 2.0$; RE = Pr, Eu)	1050–1350	3.46	1.0×10^{20}
FP-20	Fluoride phosphate	30 AlF_3–10 MgF_2–22 CaF_2–18 SrF_2–20 $Sr(PO_3)_2$–x REF_3 ($x = 0, 0.5, 2.0$; RE = Pr, Eu)	1100–1400	3.55	0.9×10^{20}

UV-3101PC). The IR spectra were measured with a Fourier transform infrared spectrophotometer (Bio-Rad FTS-40). Fluorescence spectra were obtained using a fluorescence spectrometer (Shimadzu RFPC-5001). The crystallization behavior was been studied using a digital scanning microscope (Zeiss) with an analytical data management system (Link).

3. Results

3.1. IR transparency / phonon energy

Fig. 1(a) shows the FT–IR absorbance spectra and Fig. 1(b) the FT–IR reflectance spectra of selected host glasses at 300 K. The same glasses (doped with Eu^{3+}) were used to determine the local vibration behavior around the RE ions. The excitation spectra of Eu^{3+} shown in Fig. 2 were obtained by monitoring the $^5D_0 \rightarrow {}^7F_2$ transition (emission wavelength $\lambda_{em} = 612$ nm), and were used as the starting point for the Eu^{3+} PSB interpretation. From these measurements we estimated the individual phonon energy $\hbar\omega$ for each glass family. After Todoroki et al. [14] the $\hbar\omega$ is assumed to correspond to the local vibrations including the RE ions, whose energy is less than the cut-off energy of the matrix glass (sensed by IR spectroscopy).

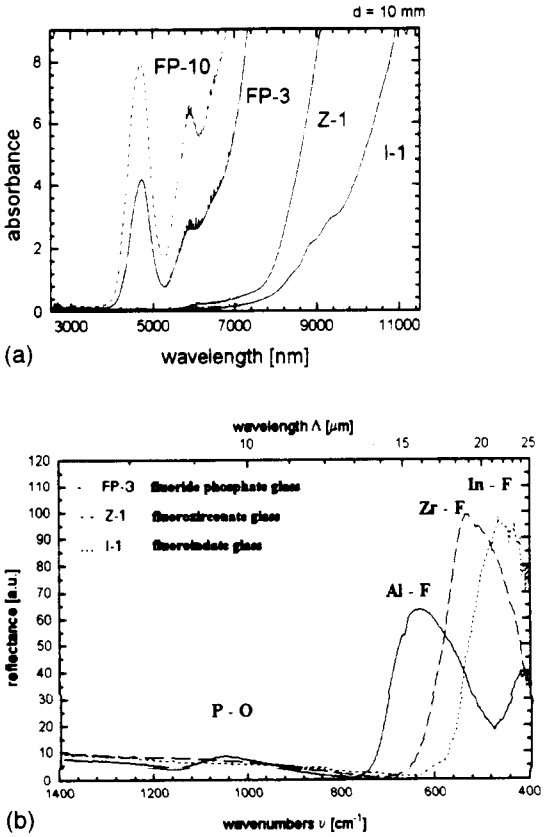

Fig. 1. (a) FT–IR absorbance spectra and (b) FT–IR reflectance spectra of selected host glasses at 300 K.

3.2. Pr^3 absorption properties / Judd–Ofelt treatment

The oscillator strength f_{exp} of transitions was estimated from the Pr^{3+} absorption spectra (e.g. Fig. 3, sample FP-3: Pr) after band separation [25] using the relationship

$$f_{exp} = \frac{mc^2}{\pi e^2} \int \sigma_{abs}(\tilde{\nu}) \mathrm{d}\tilde{\nu}, \tag{1}$$

where $\sigma_{abs}(\tilde{\nu})$ is the absorption cross section (10^{-20} cm^2) and $\tilde{\nu}$ is the wavenumber (cm^{-1}). The quantities m and e are the mass and charge of the electron, respectively, and c is the velocity of light. The cross-section $\sigma_{abs}(\tilde{\nu})$ is defined by

$$\sigma_{abs}(\tilde{\nu}) = \frac{\ln[I_0(\tilde{\nu})/I(\tilde{\nu})]}{Nt}, \tag{2}$$

where N is the number of ions per cm^3 and t is the absorption path length.

A set of f_{exp} data for each glass served as the basis for calculating the phenomenological parameters, Ω_t, using Eq. (3):

$$\begin{aligned} f_{exp}(\alpha, J, \alpha', J') &\overset{!}{=} f_{cal}(\alpha, J, \alpha', J') \\ &= \frac{8\pi^2 m \nu}{3h(2J+1)} \\ &\quad \times \left[\frac{[n^2+2]^2}{9n} \sum_{t=2,4,6} \Omega_t |\langle \alpha, J \| U^{(t)} \| \alpha', J' \rangle|^2 \right], \end{aligned} \tag{3}$$

where the symbols have conventional meanings. It should be pointed out that ν is the average fre-

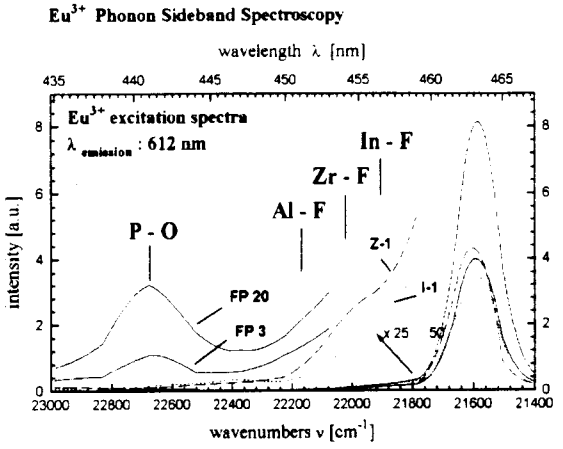

Fig. 2. Excitation spectra of Eu^{3+}-doped glasses FP-20, FP-3, Z-1 and I-1. ($\lambda_{em} = 612$ nm). The small peaks at the higher-energy side of Eu^{3+} $^7F_0 \rightarrow {}^5D_2$ are caused by PSB and give information about the phonon energy, $\hbar\omega$, in this material [14]. The positions of In–F, Zr–F, Al–F and P–O vibrations (sensed by PSB spectroscopy) are indicated.

quency. We used the tabulated Pr^{3+} matrix elements $\langle \|U^{(t)}\| \rangle$ from Weber [17]. The instrumental error of the spectrophotometric measurements was estimated to be 1%, although for extremely weak transitions this error may be as large as 10%. The number of rare earth ions per cm^3 was determined from the batch composition, melting loss and density of the glass with an accuracy of about 5%. Because of different error sources the determined data sets $f_{exp}^{(i)}$ yielded by separation of bands procedure [25] can never exactly fit the model function (3) even if the Judd–Ofelt model is correct. To use the obtained best-fit parameters for other calculations it is necessary to know their likely errors. Only together with these errors and a statistical measure for the goodness-of-fit is the interpretation of Judd–Ofelt parameters useful. The $^3H_4 \rightarrow {}^3P_2$ transition was excluded from the Ω_t estimates because of its unusual intensity behavior [19]. The remaining nine transitions in the 400–2500 nm region were used to fit three Ω_t parameters. As is well known, this overdetermined problem can be solved using a 'compromise' solution in the least-squares sense. This solution means the sum of the squares of differences between f_{exp} and f_{cal} should be minimized. Many numerical methods exist to solve this problem. We point out the necessity to integrate the 'uncertainties' of the experimental data in the fitting procedure. That is why we have chosen the 'reduced χ^2' as the minimizing quantity:

$$\chi^2 = \sum_{i=1}^{M} \left[\left[f_{exp}^{(i)} - \sum_{j=2,4,6} \left(\Omega j(i) |\langle \|U_{(i)}^{(j)}\| \rangle|^2 \right) \right] / s_i \right]^2, \quad (4)$$

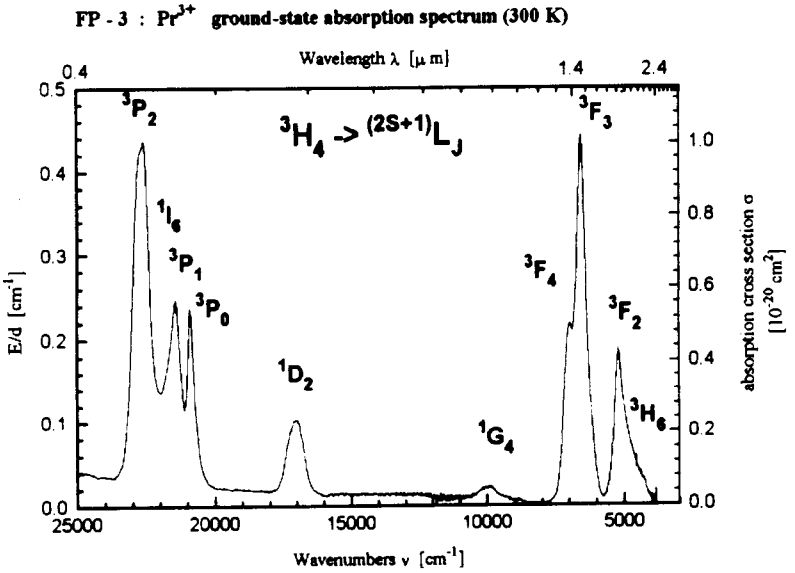

Fig. 3. Pr^{3+} absorption spectrum of glass FP-3:Pr at 300 K.

Table 2
Pr^{3+} Judd–Ofelt parameters, error values $\pm\Delta\Omega_t$ for 95% confidence, $Q = 1 - P$ (the hypersensitive transition $^3H_4 \rightarrow {}^3P_2$ is not included in the fit)

Host	Ω_2 (10^{-20} cm^2)	$\pm\Delta\Omega_2$ (10^{-20} cm^2)	Ω_4 (10^{-20} cm^2)	$\pm\Delta\Omega_4$ (10^{-20} cm^2)	Ω_6 (10^{-20} cm^2)	$\pm\Delta\Omega_6$ (10^{-20} cm^2)	χ^2	Q
FP-3	1.4	2.7	4.2	1.4	5.2	1.1	14	3×10^{-2}
FP-10	1.8	2.4	4.7	1.3	5.2	1.4	20	3×10^{-3}
FP-20	2.7	2.9	5.3	1.6	5.0	1.5	20	3×10^{-3}
Z-1	2.5	3.2	5.4	1.8	6.0	1.2	23	3×10^{-4}
I-1	3.2	3.4	4.5	1.1	6.5	1.4	39	8×10^{-6}

where ς_i is the standard deviation of the single experimental point $f_{\exp}^{(i)}$, and M is the number of transitions. It seems to be a good approach to use ς_i values equal to twice the relative deviation from band separation treatment and to add 10% for the error in the rare earth density. This means that each value of the oscillator strength is weighted by its own 'uncertainty'. We used the singular value decomposition technique to solve the mentioned fitting problem (see for example Refs. [26,27]). To estimate the goodness-of-fit of the data to the model we employed the χ^2 distribution for $M-3$ degrees of freedom. $P(m/2,\ \chi^2/2)$ is the probability that the observed χ^2 distribution will be less than a particular χ^2 for a correct model ($m = M-3$). $P(a,x)$, the incomplete gamma function, is defined by

$$P(a,x) = \frac{1}{\Gamma(a)}\int_0^x e^{-t}t^{a-1}\,dt, \quad (a>0). \tag{5}$$

where $\Gamma(a)$ is the gamma function [27]. The value $Q = 1 - P$ should be greater than about 10^{-3}, although truly wrong models give values lower than 10^{-10}. Table 2 shows the results of this treatment in terms of Ω_t, errors of Ω_t and the goodness-of-fit Q for all investigated glass systems.

The emission probability A between different RE ion levels can be estimated from parameters Ω_t using the relation

$$A(\alpha,J,\alpha',J') = \frac{64\pi^4\nu^3e^2}{3hc^3(2J+1)}\left[\frac{n[n^2+2]^2}{9}\times\sum_{t=2,4,6}\Omega_t|\langle\alpha,J\|U^{(t)}\|\alpha',J'\rangle|^2\right]. \tag{6}$$

Table 3
Constants K_1 and K_2 for estimating the refractive index $n(\lambda)$

Constant	Host				
	FP-3	FP-10	FP-20	Z-1	I-1
K_1	1.425	1.455	1.495	1.50	1.52
K_2 (nm^2)	2350	2700	3200	3500	4500

Table 4
Calculated oscillator strengths for transitions from Pr^{3+} $^1G_4$ to higher levels, $f_{cal}(^1G_4, J')$ (excited state absorption)

Sample λ ($^1G_4 \rightarrow J'$)	$f_{cal}(^1G_4, {}^1D_2)$ 1.40 μm	$f_{cal}(^1G_4, {}^3P_0)$ 0.9 1 μm	$f_{cal}(^1G_4, {}^3P_1)$ 0.87 μm	$f_{cal}(^1G_4, {}^1I_6)$ 0.85 μm	$f_{cal}(^1G_4, {}^3P_2)$ 0.79 μm	$f_{cal}(^1G_4, {}^1S_0)$ 0.27 μm
FP-3	1.3	0.3	0.4	**19**	2.0	11
FP-10	1.5	0.3	0.5	**22**	2.5	12
FP-20	2.0	0.4	0.6	**24**	3.7	14
Z-1	2.0	0.4	0.6	**26**	3.5	15
I-1	2.4	0.4	0.5	**25**	4.4	13

Table 5
Probability of spontaneous emission transitions from Pr^{3+} $^1G_4$ to J', $A(^1G_4, J')$ (1.33 μm transition for amplifier applications)

Sample λ ($^1G_4 \rightarrow J'$)	$A(^1G_4, ^3F_4)$ (s^{-1}) 3.35 μm	$A(^1G_4, ^3F_3)$ (s^{-1}) 3.3 μm	$A(^1G_4, ^3F_2)$ (s^{-1}) 2.1 μm	$A(^1G_4, ^3H_6)$ (s^{-1}) 1.85 μm	$A(^1G_4, ^3H_5)$ (s^{-1}) 1.33 μm	$A(^1G_4, ^3H_4)$ (s^{-1}) 1.01 μm
FP-3	12	2.1	1.6	69	185	17
FP-10	13	2.2	1.9	79	205	18
FP-20	14	2.3	2.2	95	220	20
Z-1	17	2.8	2.4	104	260	24
I-1	19	3.3	2.3	117	300	27

For each transition wavelength λ ($\lambda = c/\nu$) the refractive index $n(\lambda)$ was calculated using Cauchy's relation,

$$n = K_1 + (K_2/\lambda^2), \tag{7}$$

where the constants K_1 and K_2 were determined from several experimental values of $n(\lambda)$ of the investigated glasses again using a least-squares fitting procedure (Table 3).

Table 4 shows the calculated oscillator strengths of transitions from the Pr^3 $^1G_4$ level to higher levels for different host materials. These values provide

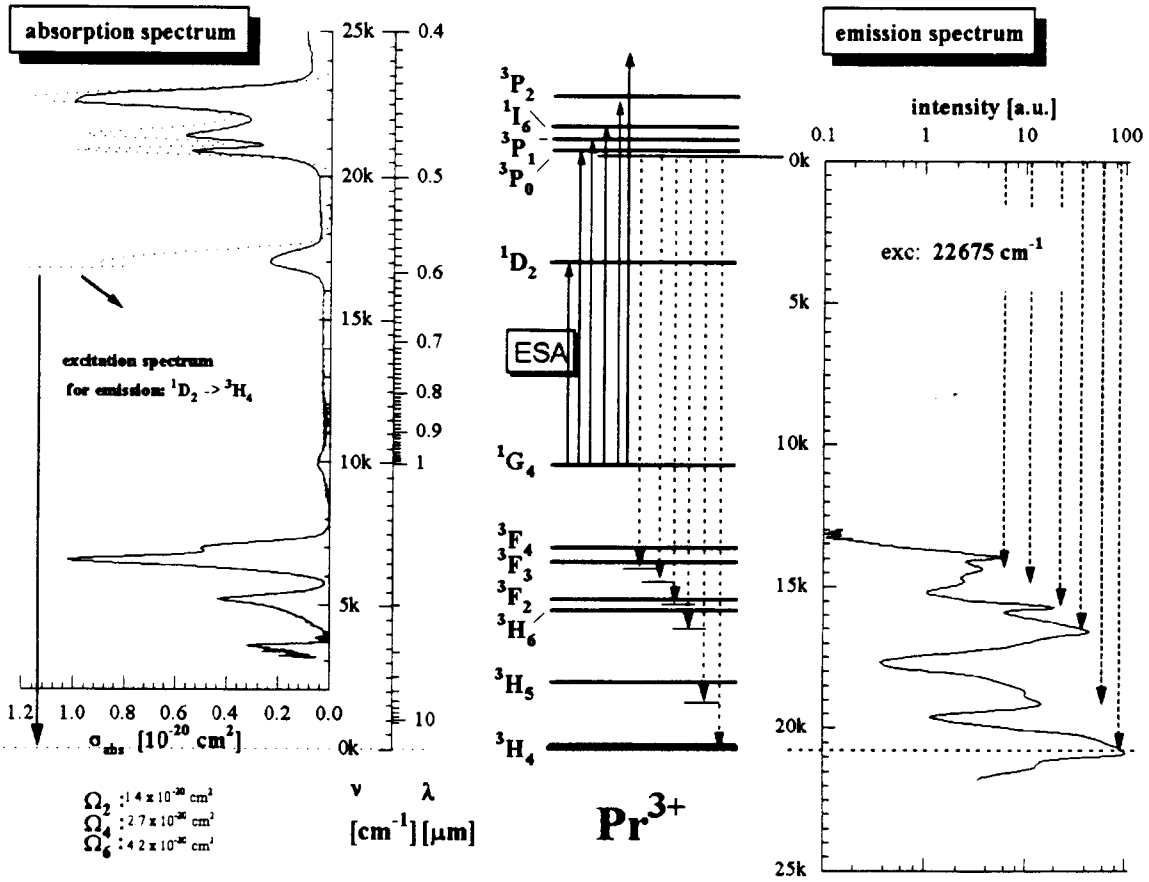

Fig. 4. Display of optical properties of the Pr^{3+}-doped FP-3 glass system. Centre: Pr^{3+} energy level diagram indicating excited state absorption (ESA) from the $^1G_4$ level and emission transitions from the $^3P_0$ level. Left: absorption and excitation spectra. Right: emission spectrum after excitation to ^3P_J levels (λ_{exc}: 441 nm).

estimates of the behavior of the excited state absorption (ESA). Table 5 presents the calculated probabilities of spontaneous emissions starting from level $^1G_4$.

The optical properties of Pr^{3+}-doped samples can easily be compared using displays such as those shown in Fig. 4. The left-hand panel shows the absorption spectrum, and the excitation spectrum monitoring the Pr^{3+} $^1D_2 \rightarrow {}^3H_4$ emission at about 636 nm. The two spectra are quite similar and support our assumption that all observed transitions belong to the Pr^{3+} level structure. The right-hand panel of Fig. 4 shows the emission behavior using an excitation wavelength of 441 nm. The detector response did not allow measurements at wavelengths $\lambda > 800$ nm.

3.3. Crystallization behavior

The fluoroindate glasses showed the highest crystallization tendency. To achieve more stable glasses we analyzed the main crystal phases. We investigated their chemical compositions using element scans for O, F, Cl, Yb, Gd, Sr, In and Ba over a 100 μm line including the fanlike crystals (Fig. 5).

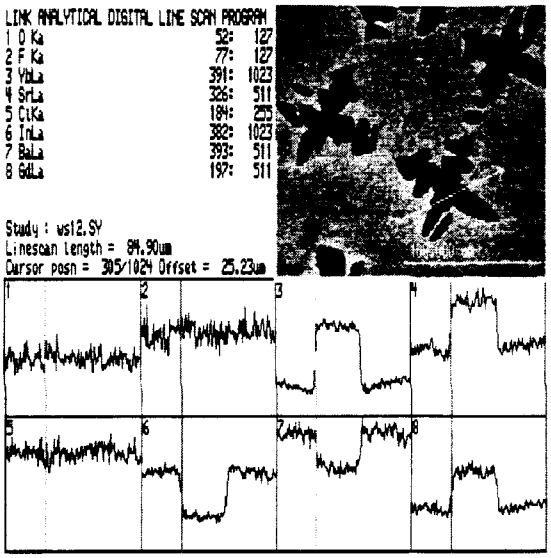

Fig. 5. Digital scanning micrograph of main crystal phases in fluoroindate glasses.

4. Discussion

4.1. IR transparency / phonon energy

Fluoride phosphate glasses, even with very low phosphate contents (FP-3, Fig. 1(a)), have strong absorptions in the 2150 cm^{-1} (4.6 μm) region due to the overtones of the P–O fundamental vibrations near 1100 cm^{-1} [28].

The fluoroindate glass obviously has the lowest absorption and scattering losses. Similar results have been reported for fluoroindate glasses with 40 mol% InF_3 contents [11]. It is well known that the maximum phonon energy $h\nu_{max}$ obtained from IR spectroscopy is higher than that derived from the PSB spectrum [14] because of differences between the local structure around the RE (sensed by Eu^{3+} PSB) and the whole glass matrix (sensed by IR).

The estimated phonon energies (Figs. 1(b) and 2) are consistent with the data reported by Todoroki et al. [14]. In terms of local structure around the RE ions in different hosts it is most likely that RE ions in the glass I-1 are surrounded by weak bonds (Ba–F or Pb–F; not In–F). On the other hand, in FP glasses the RE local vibrations are expected to couple with stronger bonds (P–O and Al–F) because of similar values of $\hbar\omega$ and $h\nu_{max}$ in these hosts (Table 6).

Fluoroindate glasses showed the lowest phonon energies and, according to Ref. [2], reduced multiphonon relaxation rates compared with those of fluorozirconates and fluoride phosphates.

Table 6
Phonon energies in different glass systems

Sample	Glass system	Phonon energy, $\hbar\omega$ (cm^{-1}) (based on PSB spectroscopy)	Maximum phonon energy, $h\nu_{max}$ (cm^{-1}) (based on IR reflectance spectroscopy)
FP 20	Fluoride phosphate	1090 ± 25	1100 ± 50
Z-1	Fluorozirconate	< 400 ± 50	550 ± 50
I-1	Fluoroindate	< 300 ± 75	450 ± 50

4.2. Pr^{3+} absorption and emission properties / Judd–Ofelt treatment

It is well known that there are problems in describing the Pr^{3+} transitions by the Judd–Ofelt theory [29], but there is a consensus about the main reason for the discrepancies: the 5d level of Pr^{3+} is low-lying and may contribute to the oscillator strength of the 4f–4f transitions. If the so-called hypersensitive transitions are not included in the calculations, the parameters behave more regularly [29,19]. As seen in Table 2, despite the exclusion of the hypersensitive transition, the Ω_2 values are poorly determined, and the errors are larger than the absolute values themselves. Fortunately, for the $^1G_4 \rightarrow {}^3H_5$ emission transition (Table 5, 1.33 μm) the $<\|U^{(2)}\|>$ matrix element is lower than the other $<\|U^{(t)}\|>$ elements and the influence of the inaccurately determined parameter Ω_2 on $A(^1G_4, {}^3H_5)$ calculations is tolerable. The same is true for the $^1G_4 \rightarrow {}^1I_6$ absorption transition (Table 4, 0.85 μm).

Fluorozirconate and fluoroindate glasses have higher oscillator strengths for $^1G_4 \rightarrow {}^1I_6$ transitions than FP glasses. This difference is important for stepwise pumping in multi-step photoexcitation applications, such as solid state 3D display devices [7,8] or up-conversion lasers. Direct excited state absorption (ESA) measurements of Pr^{3+} $^1G_4$ are difficult because of the short lifetime of the excited level $^1G_4$ and the small excited state population. These measurements are still in progress.

4.3. Crystallization behavior

The requirements for manufacturing fluoride phosphate and fluorozirconate glasses (Table 1) are less stringent than those for fluoroindates. The main problems in fluoroindate glasses are caused by fan-like crystals with sizes up to 100 μm. The element scans (Fig. 5) indicate that the crystals are composed of Sr and RE fluorides. The vitreous stability can be improved by the substitution of Sr and optimization of the RE concentrations in the batch compositions. These investigations are in progress.

5. Conclusions

In summary, the investigated fluorozirconate and fluoroindate glasses have low phonon energies below 400 cm^{-1} and have potential for active optical devices such as up-conversion lasers and 3D displays. The Pr^{3+} $^1G_4$ transition probabilities in these materials provide two-step photoexcitation. Unfortunately, the high crystallization tendency of fluoroindate glasses compares unfavorably with fluorozirconates. Fluoride phosphate glasses are not so useful for active applications because of their high phonon energies $\hbar\omega$ (caused by phosphate groups).

Parts of this work were sponsored by DAAD (grant for W. Seeber) and DFG (project Se 698/1-1; Eh 140/1-1). The authors wish to thank R. Atzrodt, T. Kittel, H. Reiß, F. Seifert and G. Völksch, University of Jena, for their assistance and helpful discussions.

References

[1] B. Jacquier, A. Remillieux, M.F. Joubert, P. Christensen and H. Poignant, J. Non-Cryst. Solids 161 (1993) 241.
[2] D.W. Hewak, R.S. Deol, J. Wang, G. Wylangowski, J.A. Mederios Neto, B.N. Samson, R.I. Laming, W.S. Brocklesby, D.N. Payne, A. Jha, M. Poulain, S. Ptero, S. Surinach and M.D. Baro, Electron. Lett. 29 (1993) 237.
[3] R.S. Quimby and B. Zheng, Appl. Phys. Lett. 60 (1992) 1055.
[4] R.G. Smart, D.C. Hanna, A.C. Tropper, S.T. Davey, S.F. Carter and D. Szebesta, Electron. Lett. 27 (1991) 1307.
[5] R.S. Deol, D.W. Hewak, S. Jordery, A. Jha, M. Poulain, M.D. Baro and D.N. Payne, J. Non-Cryst. Solids 161 (1993) 257.
[6] R.S. Deol, D.W. Hewak, J.A. Mederios Neto, B. Samson, R.S. Brown, K.P. Jedrzejewski, J. Wang, E. Taylor, R.I. Laming, G. Wylangowski and D.N. Payne, IEEE Photonics Technol. Lett. 6 (1994) 609.
[7] E.A. Downing, L. Hesselink, R.M. Macfarlane and C.P.J. Barty, Conf. on Lasers and Electro-Optics, 1994, Los Angeles, paper CMB1.
[8] E.A. Downing, L. Hesselink, W. Seeber and D. Ehrt, Glastech. Ber. Glass. Sci. Technol. 67C (1994) 354.
[9] For example, S.T. Davey, D. Szebesta, J.R. Williams, T. Whitley and R. Wyatt, J. Non-Cryst. Solids 161 (1993) 262.
[10] M. Poulain, M. Poulain, J. Lucas and P. Brun, Mater. Res. Bull. 10 (1975) 243.
[11] Y. Messaddeq, A. Delben, M. Boscolo, M.A. Aegerter, A. Soufiane and M. Poulain, J. Non-Cryst. Solids 161 (1993) 210.
[12] N. Rigout, J.L. Adam and J. Lucas, J. Non-Cryst. Solids 161 (1993) 161.
[13] W. Seeber, E.A. Downing, L. Hesselink and M.M. Fejer, Center for Nonlinear Optical Materials, Stanford University, Annual Report 1994, B.5.

[14] S. Todoroki, K. Hirao and N. Soga, J. Non-Cryst. Solids 143 (1992) 46.
[15] W.T. Carnall, P.R. Fields and K. Rajnak, J. Chem Phys. 49 (1968) 4412.
[16] W.F. Krupke, Phys. Rev. 145 (1966) 325.
[17] M.J. Weber, J. Chem. Phys. 48 (1968) 4774.
[18] J.L. Adam, W.A. Sibley and D.R. Grabbe, J. Lumin. 33 (1985) 391.
[19] M. Eyal, E. Greenberg, R. Reisfeld and N. Spector, Chem. Phys. Lett. 117 (1985) 108.
[20] J.L. Adam and W.A. Sibley, J. Non-Cryst. Solids 76 (1985) 267.
[21] Y. Ohishi, T. Kanamori, T. Nishi, Y. Nishida and S. Takahashi, 16th Int. Congr. on Glass, Madrid 1992, Bol. Soc. Esp. Ceram. Vid. 31-C 2 (1992) 73.
[22] G.H. Dieke, Spectra and Energy Levels of Rare Earths in Crystals (Interscience, New York, 1968).
[23] B.R. Judd, Phys. Rev. 127 (1962) 750.
[24] G.S. Ofelt, J. Chem. Phys. 37 (1962) 511.
[25] J. Opfermann, Non-linear Parameter Estimation Software (1985–1994), private communication.
[26] G.H. Golub and C.F. Van Loan, Matrix Computations (Johns Hopkins University Press, Baltimore, 1983).
[27] W.H. Press, B.P. Flamery, S.A. Tenkolsky and W.T. Vetterling, Numerical Recipes in Pascal (Cambridge University Press, 1989).
[28] D. Ehrt and W. Vogel, Z. Chem. 23/3 (1983) 111.
[29] R. Reisfeld and Ch. Jørgensen, Lasers and Excited States of Rare Earths (Springer, Berlin, 1977).